Phase diagram of the dissipative quantum Ising model on a square lattice

Jiasen Jin,[1] Alberto Biella,[2] Oscar Viyuela,[3,4] Cristiano Ciuti,[2] Rosario Fazio,[5,6] and Davide Rossini[7]

[1]*School of Physics, Dalian University of Technology, 116024 Dalian, China*
[2]*Laboratoire Matériaux et Phénomènes Quantiques, Université Paris Diderot, CNRS-UMR7162, F-75013 Paris, France*
[3]*Department of Physics, Massachusetts Institute of Technology, Cambridge, Massachusetts 02139, USA*
[4]*Department of Physics, Harvard University, Cambridge, Massachusetts 02318, USA*
[5]*ICTP, Strada Costiera 11, I-34151 Trieste, Italy*
[6]*NEST, Scuola Normale Superiore and Istituto Nanoscienze-CNR, I-56126 Pisa, Italy*
[7]*Dipartimento di Fisica, Università di Pisa and INFN, Largo Pontecorvo 3, I-56127 Pisa, Italy*

The competition between interactions and dissipative processes in a quantum many-body system can drive phase transitions of different order. Exploiting a combination of cluster methods and quantum trajectories, we show how the systematic inclusion of (classical and quantum) nonlocal correlations at increasing distances is crucial to determine the structure of the phase diagram, as well as the nature of the transitions in strongly interacting spin systems. In practice, we focus on the paradigmatic dissipative quantum Ising model: In contrast to the nondissipative case, its phase diagram is still a matter of debate in the literature. When dissipation acts along the interaction direction, we predict important quantitative modifications of the position of the first-order transition boundary. In the case of incoherent relaxation in the field direction, our approach confirms the presence of a second-order transition, while does not support the possible existence of multicritical points. Potentially, these results can be tested in up-to-date quantum simulators of Rydberg atoms.

Introduction. Quantum phase transitions are a cornerstone of modern statistical mechanics, originating when the ground state of a many-body system changes either continuously or abruptly, by virtue of a nonthermal control parameter [1]. This paradigm substantially changes in out-of-equilibrium conditions, where thermodynamic equilibrium is absent and all energy levels become relevant. A way to witness such nonequilibrium phenomena is, e.g., by considering an isolated quantum system and studying how it reacts to an abrupt change in one of its parameters [2]. Depending on its spectral properties, the system can locally thermalize to some equilibrium ensemble or get stuck in a more exotic many-body localized phase [3]. Alternatively, a system can be driven away from equilibrium by putting it in contact with an external environment which is at odds with the Hamiltonian dynamics (and thus does not induce thermalization). In such case the dynamics is nonunitary and, after an initial transient time, may end up in a (possibly mixed) steady state, losing track of the initial conditions. Here, we prove how the buildup of classical and quantum correlations dramatically modifies the nature of phase transitions in open systems. By employing a combination of state-of-the-art numerical approaches, we explore how these nonequilibrium systems behave near criticality. In particular, we concentrate on a prototypical quantum Ising spin-1/2 system coupled to different Markovian (memoryless) environments, whose essential properties can be captured by a Liouvillian master equation in the Lindblad form [4,5].

The amazing possibilities offered by several experimental platforms, as atomic and molecular optical systems [6], arrays of coupled QED cavities [7,8], or coupled optomechanical resonators [9], recently spurred considerable theoretical interest in the investigation of quantum matter under such a framework, including the emergence of critical phenomena and collective behaviors. In view of the complexity of the problem and the rarity of exactly solvable models [10], several analytical and numerical methods have been developed in order to deal with systems in two (or more) spatial dimensions, where critical phenomena are most likely to occur (see, for example, Refs. [11–23]). However, their general classification is still at its infancy [24].

In this Rapid Communication, we shed light on the impact of correlations in dissipative quantum phase transitions, motivated by the recent realization of a programmable quantum spin model with tunable interactions [25,26]. While on typical experimental timescales the dynamics can be safely approximated as unitary, it is possible to enhance the dissipation channel, such as to compete with the Hamiltonian dynamics, by coupling the Rydberg state to short-lived auxiliary energy levels. Through extensive numerical calculations, we highlight how the systematic inclusion of classical and quantum correlations at increasing distances is crucial to determine the structure of the phase diagram, as well as the nature of the critical boundaries in strongly interacting spin systems. In particular, we exploit cluster approaches, which have been shown to provide quantitatively accurate results in the description of the phase diagram and of critical phenomena in dissipative quantum lattice systems [14,21]. For the sake of concreteness, we frame our analysis in the paradigmatic transverse-field Ising model, with dissipation in the form of incoherent spin flips. This has been the object of intense theoretical investigation [27–31], in view of its direct

experimental simulation with interacting Rydberg atoms [32–35]. The resulting steady-state phase diagram in two dimensions raised a number of debated issues on the nature of the various transitions [12,15,36–38], and constitutes the main focus of the present Rapid Communication.

We provide evidence that, depending on the choice of the privileged axis for incoherent flips, the system exhibits either first-order or continuous transitions. When dissipation acts along the (internal) direction of spin-spin interaction, we show how the known mean-field (MF) bistability phenomena translate into first-order transitions or smooth crossovers according to the interaction strength. Our predictions quantitatively modify the phase diagram structure with respect to the one reported in the literature [12]. In the case of incoherent relaxation in the field direction, our approach does not support the possible existence of a multicritical point [38], unveiling how the emerging transition is always of second order. The effect of interactions is highlighted by characterizing the correlation length across first- and second-order transitions.

Model. The spin system Hamiltonian under investigation, ruling the coherent part of the dynamics, is

$$\hat{H} = \frac{V}{4} \sum_{\langle j,l \rangle} \hat{\sigma}_j^z \hat{\sigma}_l^z + \frac{g}{2} \sum_j \hat{\sigma}_j^x, \qquad (1)$$

where $\hat{\boldsymbol{\sigma}}_j \equiv (\hat{\sigma}_j^x, \hat{\sigma}_j^y, \hat{\sigma}_j^z)$ denote the spin-1/2 Pauli matrices on site j of a two-dimensional square lattice. The first term represents the nearest-neighbor interaction along z of strength V, while the second term accounts for a local and uniform magnetic field along the transverse direction x. We consider two different kinds of incoherent dissipative processes, acting independently and locally on each spin: These tend to flip it down either along the coupling (z), or along the field (x) direction. The full master equation governing the evolution of the system's density matrix $\rho(t)$ is

$$\partial_t \rho(t) = -i[\hat{H}, \rho] + \gamma \sum_j \left(\hat{L}_j \rho \hat{L}_j^\dagger - \frac{1}{2}\{\hat{L}_j^\dagger \hat{L}_j, \rho\} \right), \quad (2)$$

where the Lindblad jump operators on each site are all given by either $\hat{L}_j^{(z)} \equiv \frac{1}{2}(\hat{\sigma}_j^z - i\hat{\sigma}_j^y)$ or $\hat{L}_j^{(x)} \equiv \frac{1}{2}(\hat{\sigma}_j^x - i\hat{\sigma}_j^y)$, respectively. In what follows, we will be interested in the long-time limit properties of Eq. (2), which is guaranteed to reach a unique steady state (SS), $\rho_{SS} = \lim_{t \to \infty} \rho(t)$ [39]. Hereafter we adopt units of $\hbar = 1$.

Results. Let us start by taking z-oriented dissipative spin flips (model I). A simple MF approach, based on a product ansatz $\rho(t) = \otimes_j \rho_j(t)$, would decouple the Hamiltonian term $q^{-1} \sum_{\langle j,l \rangle} \hat{\sigma}_j^z \hat{\sigma}_l^z \to m^z \sum_j \hat{\sigma}_j^z$, where $m^z = \text{Tr}[\hat{\sigma}_j^z \rho_{SS}] \equiv \langle \hat{\sigma}_j^z \rangle$ is the local magnetization and q is the coordination number of the lattice, thus splitting the many-body Liouvillian into a sum of single-spin operators which can then be treated straightforwardly in a self-consistent way. Under this approximation, according to the choice of the system parameters, in some cases the solution is not unique and a bistable behavior (in which ρ_{SS} depends on the initial condition) emerges. This clearly appears in the observable m^z, as displayed by the light blue lines in the upper panels of Fig. 1, where the two branches correspond to solutions
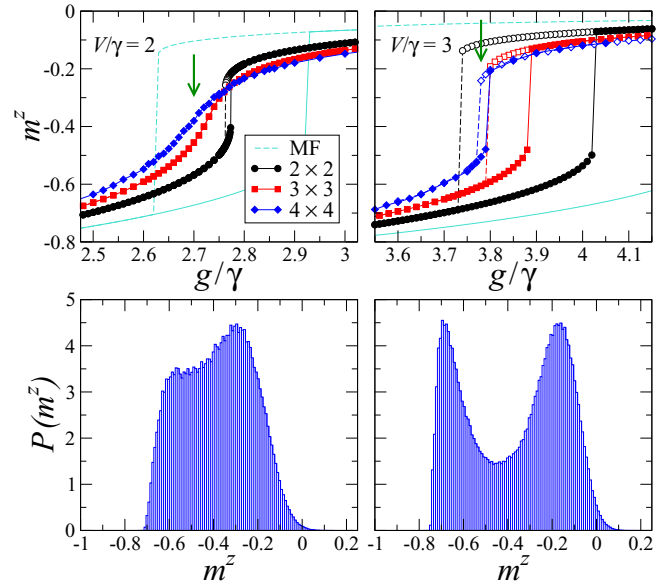

FIG. 1. Model I. Upper panels: Average steady-state magnetization m^z as a function of the transverse field g/γ, for two different values of the coupling, $V/\gamma = 2 < V_c/\gamma$ (left) and $V/\gamma = 3 \gtrsim V_c/\gamma$ (right). Light blue lines indicate the two branches of the MF solution. Symbols are results of CMF simulations for clusters of various size, as indicated in the legend. The upper/lower branch is denoted by open/solid symbols. Lower panels: Histogram of m^z sampled in time by a single quantum trajectory in a cluster with $\ell = 4$, for $V/\gamma = 2$, $g/\gamma = 2.7$ (left), and for $V/\gamma = 3$, $g/\gamma = 3.78$ (right).

obtained when sweeping from larger to smaller values of g (dashed), or conversely (continuous lines).

A more careful analysis, however, admits an exact treatment of short-range correlations that may establish within a cluster $\mathcal{C}$ of spins, while the MF is applied at the boundary of such cluster [14,40]. We performed such a cluster mean-field (CMF) study in a lattice of dimension $\ell \times \ell$, for clusters up to $\ell = 4$ [41]. The resulting magnetization is shown in the same panels, with different symbols corresponding to various cluster sizes. It appears quite neatly that the bistability region progressively shrinks when increasing ℓ, and eventually tends to disappear. Specifically, for $\ell = 4$, we can identify a threshold value of the coupling strength $V_c^{(\ell=4)}/\gamma \approx 3$, separating a region where the magnetization asymptotically exhibits a continuous behavior as g/γ is increased (top left panel, for $V/\gamma = 2$), from another one where a discontinuity in m^z spotlights the presence of a first-order transition (top right panel, for $V/\gamma = 3$, where the putative transition is located at $g_c/\gamma \approx 3.78 \pm 0.05$). However, in the latter case, for the largest available cluster size, we are still observing resilience of the system to bistability at long times, in a narrow region $3.78 \lesssim g/\gamma \lesssim 3.8$ [42]. A rough finite-size scaling of data for $\ell \leqslant 4$ suggests the onset of a critical point at a finite value ($V_c/\gamma \approx 4.05$, $g_c/\gamma \approx 4.88$), obtained by extrapolating to the thermodynamic limit (see Ref. [43]). We shall emphasize that the only other prediction available in the literature has been obtained using a variational approach [12] that locates the critical point at $V_c/\gamma = 1.4$, for which the transition is observed at $g_c/\gamma = 2.28$. Such an estimate qualitatively

agrees with our bare MF data, which slightly underestimate the location of V_c, while completely washing out correlations between the various sites. The full CMF phase diagram drawn in the V-g plane is presented in Ref. [43].

Evidence for the change of behavior when crossing V_c is also witnessed by analyzing the quantum jumps that appear when monitoring the time evolution of a single stochastic trajectory [24,45]. Once the values of the couplings are fixed, each quantum trajectory explores states with different magnetization during its dynamics. By sampling the outcomes, one obtains an histogram representing the probability to measure a given value of m^z in typical quantum optical experiments. If $V > V_c$, the system jumps abruptly from the low- to the high-density phase as g is increased [43]. By performing such a measure at the critical point g_c, the probability distribution turns out to be bimodal, since the trajectory mainly jumps between the two phases (lower right panel of Fig. 1). In particular, it is the symmetric sum on the probability distributions one would obtain in the two phases for $g < g_c$ and $g > g_c$, respectively. This reflects the fact that, at criticality, the density matrix must be the equiprobable mixture of the two phases [24]. For $V < V_c$ the system exhibits a smooth crossover between the two phases. By applying the same protocol for $g/\gamma = 2.7$ [the value for which $\partial_g m^z(g)$ is larger], the bimodal character of the distribution is smeared out, thus signaling the disappearance of the critical behavior (lower left panel of Fig. 1).

To get further insight about the impact of correlations on this physics, we employed a numerical linked cluster expansion (NLCE) [21,46]. A remarkable advantage of NLCE over other strategies is that it enables a direct access to the thermodynamic limit of an infinite number of spins, up to order R in the cluster size, by only counting cluster contributions of sizes equal to or smaller than R. Importantly, contrary to other perturbative expansions, the NLCE is not based on a perturbative parameter and the convergence of the series is controlled by the typical length scale of correlations [21,46]. In the top panel of Fig. 2, we perform a NLCE for the observable $m^z(g)$ for $V/\gamma = 2$ (crossover region). As is clear by looking at the expansion truncated at different orders (see the legend), the series does not converge in the crossover region, even when resummation techniques to speed up the convergence are employed [47]. This is due to a dramatic buildup of correlations in the crossover region, even in the noncritical case.

We further analyzed this mechanism by studying the behavior, in the transition region, of the correlation length [48]

$$(\xi^z)^2 = \frac{1}{N} \sum_{\mathbf{r},\mathbf{r}'} |\mathbf{r} - \mathbf{r}'|^2 g(\mathbf{r}, \mathbf{r}'), \tag{3}$$

where $g(\mathbf{r}, \mathbf{r}') = \langle \hat{\sigma}_{\mathbf{r}}^z \hat{\sigma}_{\mathbf{r}'}^z \rangle - \langle \hat{\sigma}_{\mathbf{r}}^z \rangle \langle \hat{\sigma}_{\mathbf{r}'}^z \rangle$ is the connected part of the two-point correlation function (specified by the coordinates $\mathbf{r}, \mathbf{r}'$) along the coupling direction, and N is the number of sites. While the above quantity refers to a correlation length calculated within a given (small) cluster, and thus cannot be directly related to the convergence of NLCE in the thermodynamic limit, it provides an intuition of the key role played by correlations close to the critical points (or their precursors). The results of calculations on a cluster of size $\ell = 4$ are
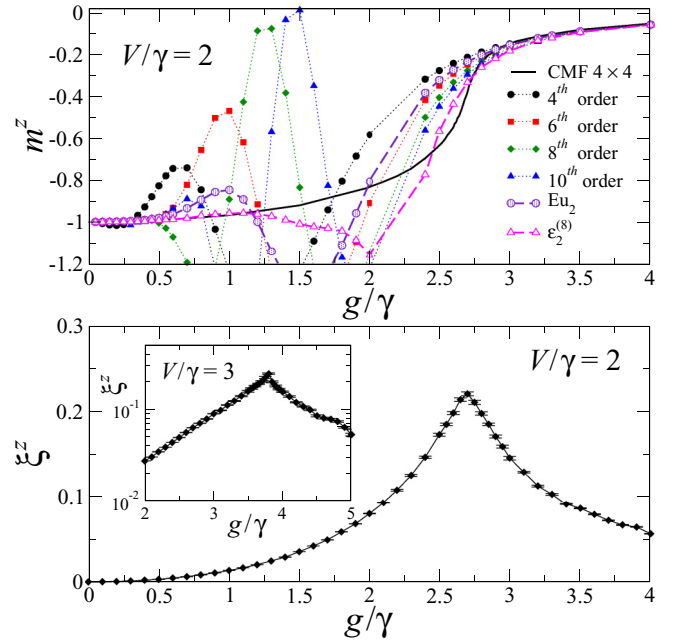

FIG. 2. Model I. Upper panel: Magnetization as a function of g/γ for $V/\gamma = 2$, evaluated with a NLCE up to tenth order and after using resummation techniques [47]. Lower panel: Correlation length ξ^z in a 4×4 cluster for $V/\gamma = 2$ (main frame, linear scale) and $V/\gamma = 3$ (inset, logarithmic scale).

displayed in the lower panel, for $V/\gamma = 2$ (main frame) and $V/\gamma = 3$ (inset), where it is shown that ξ^z undergoes a sudden increase in proximity to the transition point. This behavior also occurs in the noncritical case $V < V_c$, highlighting the importance of the exact treatment of short-range interactions even in a system that does not display a critical behavior. However, we shall stress that, in the critical case, ξ^z does not necessarily diverge in the thermodynamic limit $N \to \infty$ (as is the case for a second-order transition) and, for the clusters we were able to reach, it takes relatively small values ($\approx 10^{-1}$). This fact may hinder its experimental detection, even if such a quantity can become arbitrarily large, thus indicating the strongly correlated nature of the steady state.

We now switch to x-oriented dissipative spin flips (model II). When incoherent processes take place along the field direction (i.e., orthogonal to the spin-spin coupling), the physics of the model changes qualitatively. This scheme has been first devised and studied in one dimension, where the onset of interesting steady-state correlations and edge effects has been witnessed [49,50]. In higher dimensions and at the MF level, the system undergoes a continuous transition from a disordered paramagnetic phase ($\langle \hat{\sigma}^z \rangle = 0$) to a ferromagnetic state ($\langle \hat{\sigma}^z \rangle \neq 0$) in which the $\mathbb{Z}_2$ symmetry ($\hat{\sigma}^y, \hat{\sigma}^z) \to -(\hat{\sigma}^y, \hat{\sigma}^z)$ is spontaneously broken. A more refined treatment based on the Keldysh formalism predicts the transition to be of first order (with symmetry breaking) at sufficiently strong dissipation [36]. According to a subsequent study with a variational ansatz [38], the transition can be either continuous or first order, depending of the dissipation rate γ; the continuous and first-order transition lines meet at a tricritical point. Here, we show that systematically including the effect of correlations at an increasing distance leads to some modifications of the
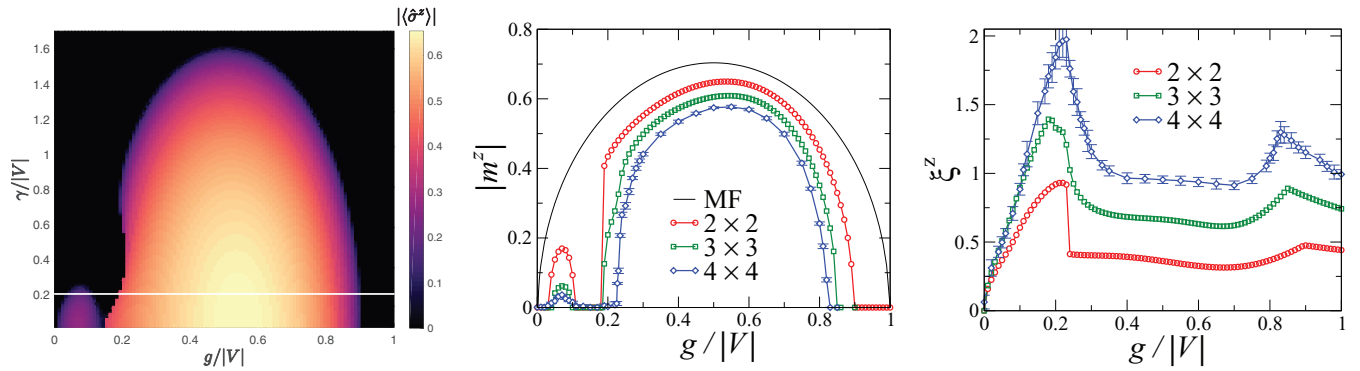
FIG. 3. Model II. Left panel: Steady-state phase diagram in the $\gamma/|V|$-$g/|V|$ plane, obtained with a $\ell = 2$ CMF approach, witnessed by the average magnetization $|m^z| = |\langle \sigma^z \rangle|$. The horizontal white line marks the cut at $\gamma/|V| = 0.2$, which has been scrutinized in the central and right panels, where we considered CMF with clusters of different sizes (see the legend). Namely, they display the behavior of the order parameter $|m^z|$ (central panel) and of the correlation length ξ^z [right panel; see Eq. (3)].

phase diagram, where only continuous transitions are present, thus excluding the possibility of a multicritical behavior. We point out that an exact treatment of short-range correlations seems to be crucial to the description of dissipative spin systems, since they have been proven to be able to substantially change the phase diagram structure [14], in accordance with alternative nonperturbative approaches based on tensor-network simulations [15].

To this aim, we study the two-dimensional phase diagram in the $\gamma/|V|$-$g/|V|$ plane, for $V < 0$. In the left panel of Fig. 3, we show the absolute value of the average magnetization $|m^z|$ as obtained with a CMF approach for $\ell = 2$. The results agree with those in Ref. [38]: For $\gamma/|V| \lesssim 0.5$ the transition is first order, otherwise it is continuous. In the central panel, we study the effect on $|m^z|$ of the exact inclusion of correlations at increasing distance, by considering clusters of size $\ell \leqslant 4$. A larger-cluster ansatz progressively smoothens the first-order jump, thus leading to a continuous transition. The lobe appearing at small g and small γ is quickly suppressed as ℓ is increased, and represents an artifact of the CMF ansatz, as also witnessed by a linear stability analysis [43,51]. The figure displays numerical results obtained for the cut at $\gamma/|V| = 0.2$, but the same conclusions apply for the whole range $\gamma/|V| \lesssim 0.5$ (not shown). In the right panel of Fig. 3, we show the behavior of the correlation length in Eq. (3) along the same cut ($\gamma/|V| = 0.2$), for different cluster sizes (namely, $\ell = 2, 3, 4$). The emergence of critical points is again witnessed by an abrupt increasing of ξ^z. In contrast to the case of the first-order transition studied in model I (Fig. 2), here the correlation length at criticality is about two orders of magnitude larger and the peak is more likely to be experimentally detected. Indeed, in the case of continuous transitions with symmetry breaking, a divergence of ξ^z in the thermodynamic limit is expected to occur.

Conclusions. We proved how the emergence of classical and quantum correlations dramatically modifies the nature of dissipative phase transitions in strongly interacting spin systems. Applying a combination of cluster methods and quantum trajectories on a testbed spin-1/2 quantum Ising model with incoherent spin flips, we demonstrated two key results. First, quantum phase bistability evolves into a crossover or a purely first-order phase transition, if short-range interactions are properly accounted for. This allowed us to precisely locate the position of the critical boundary, which has been a matter of debate in the literature. Second, certain previously thought first-order transitions are indeed second order when employing an exact treatment of interactions. This points toward excluding the presence of a multicritical behavior originated by the dissipative dynamics in the quantum Ising model. Our results also contribute to a full and comprehensive characterization of the role of correlation functions close to dissipative critical points, which represent one of the main challenges in the field of open many-body systems.

Unveiling the effect of disorder as well as disentangling the contribution of classical and quantum correlations at phase-transition points are intriguing future directions, that can be tackled within this framework. Experimentally, the fast development of quantum simulators using Rydberg atoms [25,26,32,33] stands as an exciting opportunity to test these predictions in the laboratory.

[1] S. Sachdev, *Quantum Phase Transitions* (Cambridge University Press, Cambridge, UK, 2000).

[2] A. Polkovnikov, K. Sengupta, A. Silva, and M. Vengalattore, Rev. Mod. Phys. **83**, 863 (2011).

[3] R. Nandkishore and D. A. Huse, Annu. Rev. Condens. Matter Phys. **6**, 15 (2015).

[4] H.-P. Breuer and F. Petruccione, *The Theory of Open Quantum Systems* (Oxford University Press, New York, 2002).

[5] A. Rivas and S. F. Huelga, *Open Quantum Systems. An Introduction* (Springer, Heidelberg, 2011).

[6] M. Müller, S. Diehl, G. Pupillo, and P. Zoller, Adv. At. Mol. Opt. Phys. **61**, 1 (2012).

[7] A. A. Houck, H. E. Türeci, and J. Koch, Nat. Phys. **8**, 292 (2012).

[8] M. Fitzpatrick, N. M. Sundaresan, A. C. Y. Li, J. Koch, and A. A. Houck, Phys. Rev. X **7**, 011016 (2017).

[9] M. Ludwig and F. Marquardt, Phys. Rev. Lett. **111**, 073603 (2013).

[10] M. Foss-Feig, J. T. Young, V. V. Albert, A. V. Gorshkov, and M. F. Maghrebi, Phys. Rev. Lett. **119**, 190402 (2017).

[11] P. Degenfeld-Schonburg and M. J. Hartmann, Phys. Rev. B **89**, 245108 (2014).

[12] H. Weimer, Phys. Rev. Lett. **114**, 040402 (2015).

[13] S. Finazzi, A. Le Boité, F. Storme, A. Baksic, and C. Ciuti, Phys. Rev. Lett. **115**, 080604 (2015).

[14] J. Jin, A. Biella, O. Viyuela, L. Mazza, J. Keeling, R. Fazio, and D. Rossini, Phys. Rev. X **6**, 031011 (2016).

[15] A. Kshetrimayum, H. Weimer, and R. Orus, Nat. Commun. **8**, 1291 (2017).

[16] L. M. Sieberer, M. Buchhold, and S. Diehl, Rep. Prog. Phys. **79**, 096001 (2016).

[17] A. C. Y. Li, F. Petruccione, and J. Koch, Sci. Rep. **4**, 4887 (2014); Phys. Rev. X **6**, 021037 (2016).

[18] E. Mascarenhas, arXiv:1712.00987.

[19] W. Casteels, R. M. Wilson, and M. Wouters, Phys. Rev. A **97**, 062107 (2018).

[20] R. Rota, F. Minganti, A. Biella, and C. Ciuti, New J. Phys. **20**, 045003 (2018).

[21] A. Biella, J. Jin, O. Viyuela, C. Ciuti, R. Fazio, and D. Rossini, Phys. Rev. B **97**, 035103 (2018).

[22] A. Nagy and V. Savona, Phys. Rev. A **97**, 052129 (2018).

[23] R. Rota, F. Minganti, C. Ciuti, and V. Savona, arXiv:1809.10138.

[24] F. Minganti, A. Biella, N. Bartolo, and C. Ciuti, Phys. Rev. A **98**, 042118 (2018).

[25] H. Bernien, S. Schwartz, A. Keesling, H. Levine, A. Omran, H. Pichler, S. Choi, A. S. Zibrov, M. Endres, M. Greiner, V. Vuletić, and M. D. Lukin, Nature (London) **551**, 579 (2017).

[26] A. Keesling, A. Omran, H. Levine, H. Bernien, H. Pichler, S. Choi, R. Samajdar, S. Schwartz, P. Silvi, S. Sachdev, P. Zoller, M. Endres, M. Greiner, V. Vuletić, and M. D. Lukin, arXiv:1809.05540.

[27] T. E. Lee, H. Häffner, and M. C. Cross, Phys. Rev. A **84**, 031402 (2011); Phys. Rev. Lett. **108**, 023602 (2012).

[28] T. E. Lee, S. Gopalakrishnan, and M. D. Lukin, Phys. Rev. Lett. **110**, 257204 (2013).

[29] M. Marcuzzi, E. Levi, S. Diehl, J. P. Garrahan, and I. Lesanovsky, Phys. Rev. Lett. **113**, 210401 (2014).

[30] R. Rota, F. Storme, N. Bartolo, R. Fazio, and C. Ciuti, Phys. Rev. B **95**, 134431 (2017).

[31] D. Roscher, S. Diehl, and M. Buchhold, arXiv:1803.08514 [Phys. Rev. A (to be published)].

[32] C. Carr, R. Ritter, C. G. Wade, C. S. Adams, and K. J. Weatherill, Phys. Rev. Lett. **111**, 113901 (2013).

[33] V. Lienhard, S. de Léséleuc, D. Barredo, T. Lahaye, A. Browaeys, M. Schuler, L.-P. Henry, and A. M. Läuchli, Phys. Rev. X **8**, 021070 (2018).

[34] S. de Léséleuc, S. Weber, V. Lienhard, D. Barredo, H. P. Büchler, T. Lahaye, and A. Browaeys, Phys. Rev. Lett. **120**, 113602 (2018).

[35] D. Barredo, V. Lienhard, S. de Léséleuc, T. Lahaye, and A. Browaeys, Nature (London) **561**, 79 (2018).

[36] M. F. Maghrebi and A. V. Gorshkov, Phys. Rev. B **93**, 014307 (2016).

[37] D. C. Rose, K. Macieszczak, I. Lesanovsky, and J. P. Garrahan, Phys. Rev. E **94**, 052132 (2016).

[38] V. R. Overbeck, M. F. Maghrebi, A. V. Gorshkov, and H. Weimer, Phys. Rev. A **95**, 042133 (2017).

[39] S. G. Schirmer and X. Wang, Phys. Rev. A **81**, 062306 (2010).

[40] A. Tomadin, V. Giovannetti, R. Fazio, D. Gerace, I. Carusotto, H. E. Türeci, and A. Imamoglu, Phys. Rev. A **81**, 061801 (2010).

[41] For clusters of size $\ell = 2$ we were able to diagonalize exactly the Liouvillian. For $\ell = 3$ the steady state has been obtained by simulating the time evolution of the full master equation with a fourth-order Runge-Kutta algorithm. For $\ell = 4$ we resorted to quantum trajectories. Unless specified, data presented in this Rapid Communication have been obtained by averaging over $\gtrsim 500$ trajectories.

[42] We note a systematic increasing of the bistability range as V grows. As a result, in such case the size of the cluster needed to kill this MF artifact becomes bigger. The convergence time of the simulations also increases close to the critical point [43], due to the reduction of the Liouvillian gap which determines the longest timescale for approaching the steady state [44].

[43] See Supplemental Material at http://link.aps.org/supplemental/10.1103/PhysRevB.98.241108 for details on the phase diagram for model I, the temporal behavior of the magnetization and of a single quantum trajectory close to a first-order transition, and a stability analysis for model II, close to the emerging continuous transition.

[44] K. Macieszczak, M. Guţă, I. Lesanovsky, and J. P. Garrahan, Phys. Rev. Lett. **116**, 240404 (2016).

[45] F. Vicentini, F. Minganti, R. Rota, G. Orso, and C. Ciuti, Phys. Rev. A **97**, 013853 (2018).

[46] M. Rigol, T. Bryant, and R. R. P. Singh, Phys. Rev. Lett. **97**, 187202 (2006); B. Tang, E. Khatami, and M. Rigol, Comput. Phys. Commun. **184**, 557 (2013).

[47] We applied a Euler transformation at order Eu_2, and Wynn's algorithm $\epsilon_2^{(8)}$, on top of the bare expansion up to $R = 10$. For details about this resummation technique, see Ref. [46].

[48] M. Campostrini, A. Pelissetto, and E. Vicari, Phys. Rev. B **89**, 094516 (2014).

[49] C.-E. Bardyn and A. Imamoglu, Phys. Rev. Lett. **109**, 253606 (2012).

[50] C. Joshi, F. Nissen, and J. Keeling, Phys. Rev. A **88**, 063835 (2013).

[51] A. Le Boité, G. Orso, and C. Ciuti, Phys. Rev. Lett. **110**, 233601 (2013); Phys. Rev. A **90**, 063821 (2014).